


RESEARCH ARTICLE

Magnetic resonance evidence of increased iron content in subcortical brain regions in asymptomatic Alzheimer's disease

Qixiang Lin¹ | Salman Shahid¹ | Antoine Hone-Blanchet¹ | Shuai Huang² |
Junjie Wu² | Aditya Bisht¹ | David Loring¹ | Felicia Goldstein^{1,3} |
Allan Levey^{1,3} | Bruce Crosson^{1,2} | James Lah^{1,3} | Deqiang Qiu^{2,3,4} 

¹Department of Neurology, School of Medicine, Emory University, Atlanta, Georgia, USA

²Department of Radiology and Imaging Sciences, School of Medicine, Emory University, Atlanta, Georgia, USA

³Goizueta Alzheimer's Disease Research Center, Emory University, Atlanta, Georgia, USA

⁴Joint Department of Biomedical Engineering, Emory University and Georgia Institute of Technology, Atlanta, Georgia, USA

Correspondence

James Lah, Emory Brain Health Center,
12 Executive Park Dr., NE Atlanta, GA 30329,
USA.
Email: jlah@emory.edu

Deqiang Qiu, 1364 Clifton Road NE, Suite
CG06, Atlanta, GA 30322, USA.
Email: deqiang.qiu@emory.edu

Funding information

Goizueta Foundation; National Institutes of Health, Grant/Award Numbers: R01AG070937, R01AG072603, R21AG064405, P30AG066511

Abstract

While iron over-accumulation has been reported in late stage Alzheimer's disease (AD), whether this occurs early in the asymptomatic stage of AD remains unknown. We aimed to assess brain iron levels in asymptomatic AD using quantitative MR relaxometry of effective transverse relaxation rate ($R2^*$) and longitudinal relaxation rate ($R1$), and recruited 118 participants comprised of three groups including healthy young participants, and cognitively normal older individuals without or with positive AD biomarkers based on cerebrospinal fluid (CSF) proteomics analysis. Compared with the healthy young group, increased $R2^*$ was found in widespread cortical and subcortical regions in the older groups. Further, significantly higher levels of $R2^*$ were found in the cognitively normal older subjects with positive CSF AD biomarker (i.e., asymptomatic AD) compared with those with negative AD biomarker in subcortical regions including the left and right caudate, left and right putamen, and left and right globus pallidus ($p < .05$ for all regions), suggesting increased iron content in these regions. Subcortical $R2^*$ of some regions was found to significantly correlate with CSF AD biomarkers and neuropsychological assessments of visuospatial functions. In conclusion, $R2^*$ could be a valuable biomarker for studying early pathophysiological changes in AD.

KEYWORDS

aging, Alzheimer's disease, beta-amyloid, grey matter, iron deposition, quantitative magnetic resonance imaging, subcortical

1 | INTRODUCTION

Alzheimer's disease (AD) poses enormous economic and societal burdens with a projected increase in cost to \$1.2 trillion by 2050 (World Health Organization, 2015). While the deposition of A β plaques and neurofibrillary tangles of hyperphosphorylated tau proteins in the brain are two hallmarks of AD (Jack et al., 2018; Selkoe, 1991), recent

clinical trials (Doody et al., 2014; Salloway et al., 2014) targeting the reduction of A β burden have failed to show positive effects on cognitive outcomes despite evidence of successful reduction of A β burden in the brain. It is also known that cognitively normal elderly patients with positive cerebrospinal fluid (CSF) or positron emission tomography (PET) biomarkers of brain A β deposition can remain asymptomatic for decades, and some may never become symptomatic (Chetelat

This is an open access article under the terms of the [Creative Commons Attribution-NonCommercial](https://creativecommons.org/licenses/by-nc/4.0/) License, which permits use, distribution and reproduction in any medium, provided the original work is properly cited and is not used for commercial purposes.

© 2023 The Authors. *Human Brain Mapping* published by Wiley Periodicals LLC.

et al., 2013; Vandenbergh et al., 2013). A β pathology alone is not sufficient to cause cognitive impairment as evidenced by the fact that about 30% of cognitively normal subjects older than 80 years have severe A β pathology (Fagan et al., 2007; Mintun et al., 2006; Rowe et al., 2013; Shaw et al., 2009). These findings and others suggest that other pathologies beyond A β and Tau are important in driving the neuronal damages that eventually lead to cognitive impairments.

The accumulation of iron in the brain is a hallmark of aging and neurodegenerative diseases (Daugherty & Raz, 2015; Ward et al., 2014). While iron is essential for supporting many normal functions such as oxygen transportation, synthesis of adenosine triphosphate (ATP) in mitochondria (Mills et al., 2010), DNA replication (Ward et al., 2014), and the formation of myelin (Todorich et al., 2009), excessive accumulation of intracellular non-heme iron in the brain can promote oxidative stress and trigger a cascade of neuroinflammatory and other pathological processes that will eventually lead to neuronal damage (Haider et al., 2014; Mills et al., 2010). Iron is closely linked to AD pathology: a meta-analysis of 300 postmortem AD cases showed elevated brain iron in cortical regions although the elevation was variable among regions (Tao et al., 2014). Postmortem studies have also shown that high iron concentrations are associated with amyloid plaques and neurofibrillary tangles in AD (Collingwood et al., 2005; Smith et al., 1997; Ward et al., 2014), and neuroinflammation and activation of microglia have also been associated with elevated iron in AD (Zeineh et al., 2015). Several previous *in vivo* studies using MR measures sensitive to iron, such as transverse relaxation rate R2* (Haacke et al., 2005; Langkammer et al., 2010), have found increased iron content in both healthy aging (Aquino et al., 2009; Ghadery et al., 2015; Langkammer et al., 2010; Lin et al., 2019; Sedlacik et al., 2014), and in the symptomatic stages of AD (Ayton et al., 2020; Bulk et al., 2018; Damulina et al., 2020; Spotorno et al., 2020; van Bergen et al., 2016). However, it is unclear whether brain iron over-accumulation occurs early in the asymptomatic stage of AD when the participants have accumulated positive CSF biomarker of AD pathology but are cognitively normal based on their neuropsychological assessments.

In this study, we performed a cross-sectional study comparing cortical and subcortical MR relaxometry in 118 participants comprised of three groups: healthy young (HY) adults, cognitively normal older participants with negative CSF biomarkers of AD (CN $-$) and cognitively normal older participants with positive CSF biomarkers of AD (CN $+$). Besides studying MR effective transverse relaxation R2*, we also studied MR longitudinal relaxation rate R1 (the inverse of T1) since R1 has been previously shown to be sensitive to tissue loss and myelination (Callaghan et al., 2014; Lutti et al., 2014; Sigalovsky et al., 2006; Stuber et al., 2014; Yeatman et al., 2014). Comparisons between HY and CN $-$ allow us to study the differences in R1 and R2* associated with healthy aging, while comparisons between CN $-$ and CN $+$ could suggest early brain microstructural differences associated with asymptomatic AD pathology compared to controls. We hypothesized that (1) there are significant differences in quantitative R2* and R1 values between the three groups; (2) the CN $+$ group would show a higher R2* value indicating higher iron deposition level compared

with CN $-$ and HY groups and these values are associated with neuropsychological performance.

2 | MATERIALS AND METHODS

2.1 | Participants

A total of 118 subjects were included in the present study, comprised of 39 HY adult participants (mean \pm SD age: 26.6 \pm 5.1, 14 males), 61 CN $-$ (67.4 \pm 4.2 years; 9 males) and 18 CN $+$ (70.6 \pm 6.4, years, 2 males). Members of the CN $-$ and CN $+$ groups were participants in the ongoing Emory Healthy Brain Study (EHBS; Goetz et al., 2019). All participants provided written informed consent under a protocol that was approved by the Institutional Review Board of Emory University. All participants were cognitively normal individuals, and participants with prior history of neurological disorders were excluded from enrollment in the EHBS such as stroke, epilepsy, brain tumors, or clinical history of Parkinson's disease.

2.2 | Neuropsychological assessment

From a larger cognitive assessment battery administered to each participant, we selected the following tests for further analysis because of their significant association with CSF biomarkers in a large pool of EHBS participants (Goetz et al., 2019): Montreal Cognitive Assessment (MoCA; Nasreddine et al., 2005) for overall cognitive performance; Rey Complex Figure Test (RCFT; Osterrieth, 1944) for memory and visuospatial functions; Judgment of Line Orientation (JoLO; Benton et al., 1994) for visuospatial functions. The RCFT test includes three subdomains: immediate recall score, delay recall score and copy accuracy score of Rey Figure.

2.3 | CSF biomarkers collection and analysis

Lumbar punctures were performed both in CN $-$ and CN $+$ participants at the L3-4 or L4-5 interspace with a 24-g Sprotte atraumatic spinal needle. We did not perform CSF collections in the HY group. CSF samples were collected into polypropylene transfer tubes and frozen on dry ice within 1 h after collection. Aliquots (0.5 mL) were prepared from these samples after thawing (1 h) at room temperature and gentle mixing. Following a single freeze-thaw cycle, amyloid- β 1-42 (A β ₄₂), total tau (T-tau), and tau phosphorylated at threonine 181 (pTau) were measured using the multiplex xMAP Luminex platform (Luminex Corp., Austin, Texas, USA) with Innogenetics (INNO-BIA AlzBio3; Ghent, Belgium) immunoassay kit-based reagents. All assays were performed in a single laboratory (AKESogen, Peachtree Corners, Georgia, USA). Subsequent aliquots were stored in bar code-labeled FluidX 0.9 mL polypropylene vials (Brooks Life Sciences, Chelmsford, Massachusetts, USA) at -80°C . The CSF biomarkers in the current study include A β ₄₂, T-tau, phosphorylated Tau (pTau), T-

tau/A β_{42} ratio and pTau/A β_{42} ratio. T-tau/A β_{42} ratio was calculated as an indicator of A β and tau burden. A local cutoff of T-tau/A β_{42} ratio >0.18 for AD-biomarker positivity were established by analyzing results from 1298 individuals including those diagnosed with MCI or dementia due to AD ($n = 345$), other non-AD dementia ($n = 37$), and normal controls ($n = 916$). Hence, the cognitively normal older participants with T-tau/A β_{42} ratio >0.18 were classified as having positive AD pathology therefore included in the CN+ group, while others were classified as having negative AD pathology and included in the CN- group.

2.4 | MRI acquisitions

All scans were performed on a Siemens Magnetom Prisma 3T scanner with a 32-channel phased-array head coil at the Brain Health Center of Emory University. A variable flip-angle multi-echo 3D Spoiled Gradient Echo (ME-GRE) protocol was performed with the following parameters: voxel size = $0.72 \times 0.72 \times 1.44 \text{ mm}^3$, TR = 37 ms, 5 echoes with TE = 6.61, 12.85, 19.09, 25.33, 31.57 ms at two flip angles (FA): 15° and 40°. The multi-echo variable flip-angle approach extends a previous method (Deoni et al., 2003) to allow for simultaneous quantification of both quantitative R1 and R2*. To account for inhomogeneity in B1 transmit field, a double-angle technique using a 2D echo-planar-imaging (EPI) sequence was performed to estimate the radiofrequency transmission field (B1-transmit) with the following parameters: flip angle 30° and 60°, TR = 10,000 ms, TE = 23 ms, voxel size = $3.5 \times 3.5 \times 4.2 \text{ mm}^3$. 3D T1-weighted (T1w) image were acquired using a Magnetization Prepared Rapid Gradient Echo (MPRAGE) sequence with the following parameters: TR = 2300 ms, TE = 2.96 ms, TI = 900 ms, flip angle = 9°, 208 sagittal slices with slice thickness = 1 mm, in-plane matrix size = 256×240 , isotropic voxel size.

2.5 | Image preprocessing and statistical analyses

Following the quantification of R2* and R1 map as detailed below, we performed surface-based analysis for the cerebral cortex because surface-based analysis has been shown to increase sensitivity to aging effects and reduce confounds due to smoothing across the sulcus in volume-based analysis. For deep brain regions including the caudate, the putamen, the globus pallidum, the nucleus accumbent, the thalamus, the hippocampus, and the amygdala, we performed region of interest-based analysis.

2.5.1 | Quantification of R2* and R1

The R2* value of each voxel was calculated by fitting a mono-exponential function to the magnitude signals of the 5 echoes from the ME-GRE for both acquisitions with flip angle 15° and 40°, respectively and then averaged. To calculate quantitative R1, we extended

the DESPOT1 method (Deoni et al., 2003) to the multi-echo data. More specifically, R1 values were calculated for each of the five echoes from the FA = 15° and FA = 40° acquisitions using the DESPOT1 method, and then a weighted average of the estimated R1 values across the 5 echoes was then calculated (Figure 1). In order to account to inhomogeneous B1-transmit field, we performed B1-transmit field mapping using a fast double flip-angle methods (Cunningham et al., 2006), and the estimated flip angle mapping was used in the calculation of R1. More details of the calculation of quantitative R2* and R1 are provided in the Supporting Information.

2.5.2 | Surface-based analysis of R2* and R1 in the cortex

Instead of using traditional volume-based approaches, we used surface-based analysis for the cortex, which has been shown to reduce the partial volume effect, reduce the bias and variance contaminated by smoothing, and enable more precise spatial localization of regions of effect in the cortical area. Cortical surface reconstruction and tissue segmentation were performed on the T1w images using the Freesurfer pipeline (v6.0, Massachusetts General Hospital, MA, USA, <http://surfer.nmr.mgh.harvard.edu>). Then, the R2* and R1 maps of each participant were coregistered to the individual T1w image using an affine transformation derived from the boundary-based registration between the magnitude image of flip-angle 40° and T1w image. Both quantitative R2* and R1 values of the cortex were then projected to the cortical surface generated by Freesurfer by sampling along the mid-surface estimated from the center of the cortical ribbon based on the inner and outer surfaces. Then, all surface-based R2* and R1 maps were smoothed with a 3-mm full width half maximum (FWHM) 2D kernel to improve the reliability and detectability of effects for the analysis. Surface-based one-way ANOVA analysis was performed for the cortical regions to detect group differences between HY, CN-, and CN+, followed by post hoc analyses to detect the pair-wise difference in R2* and R1 values between groups with a statistical threshold at $p < .05$ after false discovery rate (FDR) correction for multiple comparisons. General linear modeling (GLM) was then applied to study differences in both R2* and R1 in the cortical surface between the CN- and CN+ groups with age and sex as covariates, followed by an FDR correction at corrected $p < .05$.

2.5.3 | ROI-based analysis of R2* and R1 in the deep brain regions

For the subcortical regions, the mean R2* and R1 values of each anatomical region were calculated by using the corresponding Freesurfer segmentation outputs from the 3D T1w images as masks. A total of seven subcortical regions from each hemisphere (a total of 14 regions) were considered, including the left and right thalamus, caudate nucleus, putamen, globus pallidus, hippocampus, amygdala, and nucleus accumbens. Similar to the surface-based analysis, one-way

Brief overview of the data preprocessing

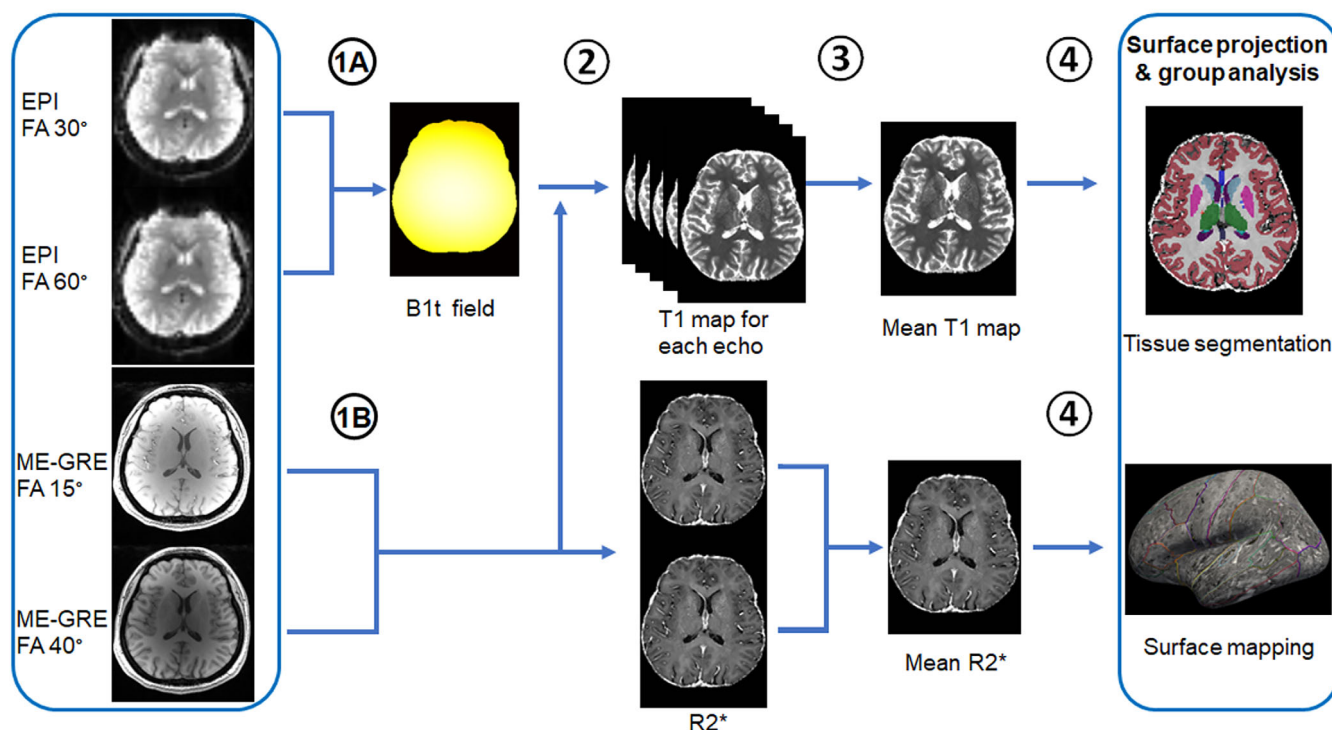


FIGURE 1 Brief overview of data preprocessing workflow. (1A) The B1 transmission (B1t) field was calculated from the double flip angle (FA) fast echo-planar-imaging sequence data. (1B) For each flip angle, R2* maps were acquired by mono-exponential fitting (2) Combined with the B1 transmission field, T1/R1 maps were calculated from the two flip angles ME-GRE sequence data using the variable-flip angles R1 mapping method and (3) the mean T1(R1) map were obtained by weighted average from 5 echoes, mean R2* images were averaged from FA 15° and FA 40°. The calculation details of quantitative R2* and R1 are provided in the Supporting Information. (4) Cortical/subcortical regions and cortical surfaces were derived from the tissue segmentation and surface reconstruction of MPRAGE data and then R1 and R2* maps were projected onto the cortical surface for further statistical analysis

ANOVA was first performed to determine the group effects in the subcortical regions followed by post hoc analysis to detect the pairwise difference between the groups with a statistical threshold at $p < .05$ after FDR correction for multiple comparisons. To further analyze specific differences in both R2* and R1 in the subcortical regions between the CN– and CN+ groups, we applied additional GLM analyses with the age and sex as covariates followed by an FDR correction at corrected $p < .05$. Brain regions that showed significant differences among the three groups, associations between R2* or R1, each of the CSF biomarkers, and neuropsychological performance were further examined using partial correlation analysis controlling for age in the CN– and CN+ groups.

3 | RESULTS

3.1 | Demographic results

The age of CN+ group is slightly higher than CN– group ($p = .025$) as expected due to the higher prevalence of positive AD pathology with increasing age, therefore we included age as a covariate in all our

subsequent analyses when appropriate. Two-sample *T*-test showed no significant differences in years of education or cognitive performances between CN– and CN+ groups (Table 1).

3.2 | Group comparisons in quantitative R2*

One-way ANOVA analysis showed significantly different R2* between the HY, CN– and CN+ groups ($p < .05$, FDR corrected) in most of the subcortical regions bilaterally, including the caudate nucleus, putamen, pallidum, hippocampus, amygdala, and nucleus accumbens, possibly due to dominating effects of aging between HY and the two older groups (CN– and CN+). There were no significant differences in either the left or right thalamus in the ANOVA analyses including all three groups (Figure 2). More interestingly, compared with the CN– group, the CN+ group showed significantly increased R2* values ($p < .05$, FDR corrected) in the right caudate, right and left putamen and the right and left pallidum after controlling for the effect of age and sex (Table 2; Figure 2).

Surface-based analysis for the cortex demonstrated wide-spread differences in R2* values between HY, CN– and CN+ across cortical

Group	Young	CN–	CN+	p-Value
Number	39	61	18	N/A
Age	26.6 ± 5.1	67.4 ± 4.2	70.6 ± 6.4	<10 ^{−6a}
Gender (M/F)	14/25	14/47	2/16	NS
Education	-	16.47 ± 2.31	17.50 ± 2.34	NS
Rey-O copy	-	31.37 ± 3.56	30.83 ± 4.17	NS
Rey-O immediate	-	17.09 ± 6.66	15.36 ± 5.15	NS
Rey-O delayed	-	16.16 ± 6.48	14.63 ± 6.95	NS
JoLO total	-	24.84 ± 3.58	24.53 ± 3.09	NS

TABLE 1 Demographic characteristics and neuropsychiatric data of participants

Note: Data are presented as the mean ± standard deviation (SD); HY: Healthy young group; CN–: cognitively normal old with CSF biomarker negative; CN+: cognitively normal old with CSF biomarker positive; Rey-O copy: Copy accuracy score of Rey Figure Test; Rey-O immediate: Immediate free recall score of Rey Figure Test; Rey-O delayed: Delayed recall score of Rey Figure Test; JoLO: Judgment of Line Orientation test.

^ap value from one-way ANOVA, the p value of the 2-sample t-test between CN– and CN+ is 0.025;

N/A: not applicable; NS: no significant differences.

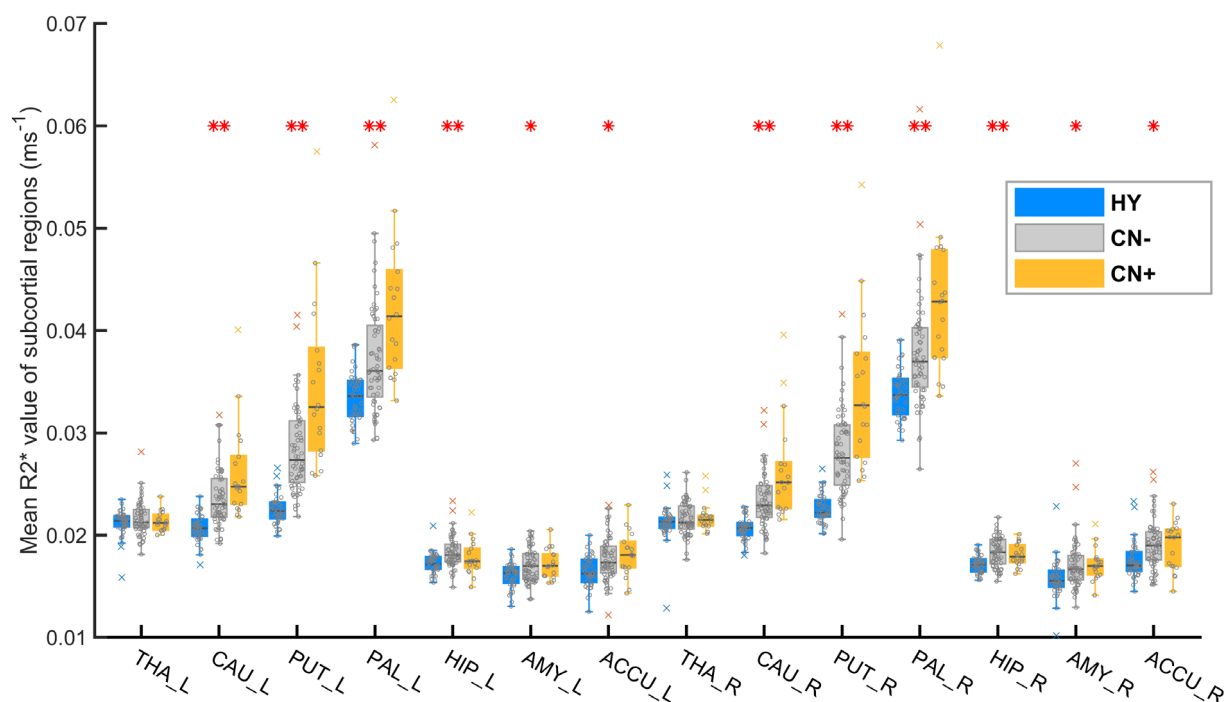


FIGURE 2 Boxplot of mean R2* value of subcortical regions. The median of R2* values of each region is displayed by the central line within the box. Box edges represent the 25th and 75th percentile values for each group. Outliers are displayed by cross markers. Blue color represents the healthy young (HY) group; Grey color represents the CN– group and orange color represents the CN+ group. R2* values are given in kilohertz (ms^{−1}); * indicates the significance level of one-way ANOVA at $p < .01$; ** indicates the significance level at $p < .001$. All these results were corrected by using FDR under $p < .05$; L: left hemisphere; R: right hemisphere; THA: thalamus; CAU: caudate; PUT: putamen; PAL: pallidum; HIP: hippocampus; AMY: amygdala; ACCU: accumbens

regions ($p < .01$, FDR corrected), again possibly due to dominating effects of aging between HY and the older two groups (CN– and CN+; Figure 3). Post hoc analysis showed that there were significantly increased R2* values bilaterally in the frontal lobes, parietal lobes, and some portions of the temporal lobes in CN– and CN+ compared with the HY group. No significant difference in R2* was found between the CN– and CN+ groups in the cortical regions after controlling for the effects of age and sex and multiple comparison correction.

3.2.1 | Correlation between R2*, CSF biomarkers, and neuropsychological assessments

In the older groups (combining the CN– and CN+ groups), significant correlations between the R2* and the CSF biomarkers was found in several basal ganglia areas after controlling for the effects of age (Figure 4). R2* values were significantly correlated with CSF T-tau/A β ratio in the left putamen ($r = 0.326$, uncorrected $p = .0036$, FDR-

TABLE 2 R^2 value for subcortical regions in HY, CN–, and CN+ (Unit: ms^{-1})

Regions	HY	CN–	CN+	p Value for ANOVA for 3 groups	p Value for CN– vs. CN+
Left-Caudate	0.021 ± 0.0014	0.024 ± 0.0029	0.026 ± 0.0047	$<0.00001^{**}$	0.0323^*
Left-Putamen	0.023 ± 0.0015	0.028 ± 0.0042	0.035 ± 0.0083	$<0.00001^{**}$	0.0003^{**}
Left-Pallidum	0.033 ± 0.0025	0.037 ± 0.0054	0.042 ± 0.0073	$<0.00001^{**}$	0.0062^{**}
Left-Hippocampus	0.017 ± 0.0010	0.018 ± 0.0015	0.018 ± 0.0017	0.00067^{**}	NS
Left-Amygdala	0.016 ± 0.0012	0.017 ± 0.0017	0.017 ± 0.0014	0.00258^{**}	NS
Left-Accumbens	0.016 ± 0.0015	0.018 ± 0.0021	0.018 ± 0.0022	0.00237^{**}	NS
Right-Caudate	0.021 ± 0.0012	0.023 ± 0.0027	0.026 ± 0.0049	$<0.00001^{**}$	0.0044^{**}
Right-Putamen	0.023 ± 0.0014	0.028 ± 0.0042	0.034 ± 0.0076	$<0.00001^{**}$	0.0004^{**}
Right-Pallidum	0.034 ± 0.0024	0.038 ± 0.0054	0.043 ± 0.0079	$<0.00001^{**}$	0.0050^{**}
Right-Hippocampus	0.017 ± 0.0009	0.018 ± 0.0014	0.018 ± 0.0011	0.00004^{**}	NS
Right-Amygdala	0.016 ± 0.0018	0.017 ± 0.0023	0.017 ± 0.0016	0.00628^{**}	NS
Right-Accumbens	0.018 ± 0.0018	0.019 ± 0.0024	0.019 ± 0.0024	0.00236^{**}	NS

Note: All the values present as mean \pm SD; R^2 values are given in kilohertz (ms^{-1}); HY: healthy young; CN–: cognitively normal older with CSF biomarkers negative; CN+: cognitively normal older with CSF biomarkers positive.

*Indicates $p < .05$; **Indicates $p < .01$; NS: no significant differences.

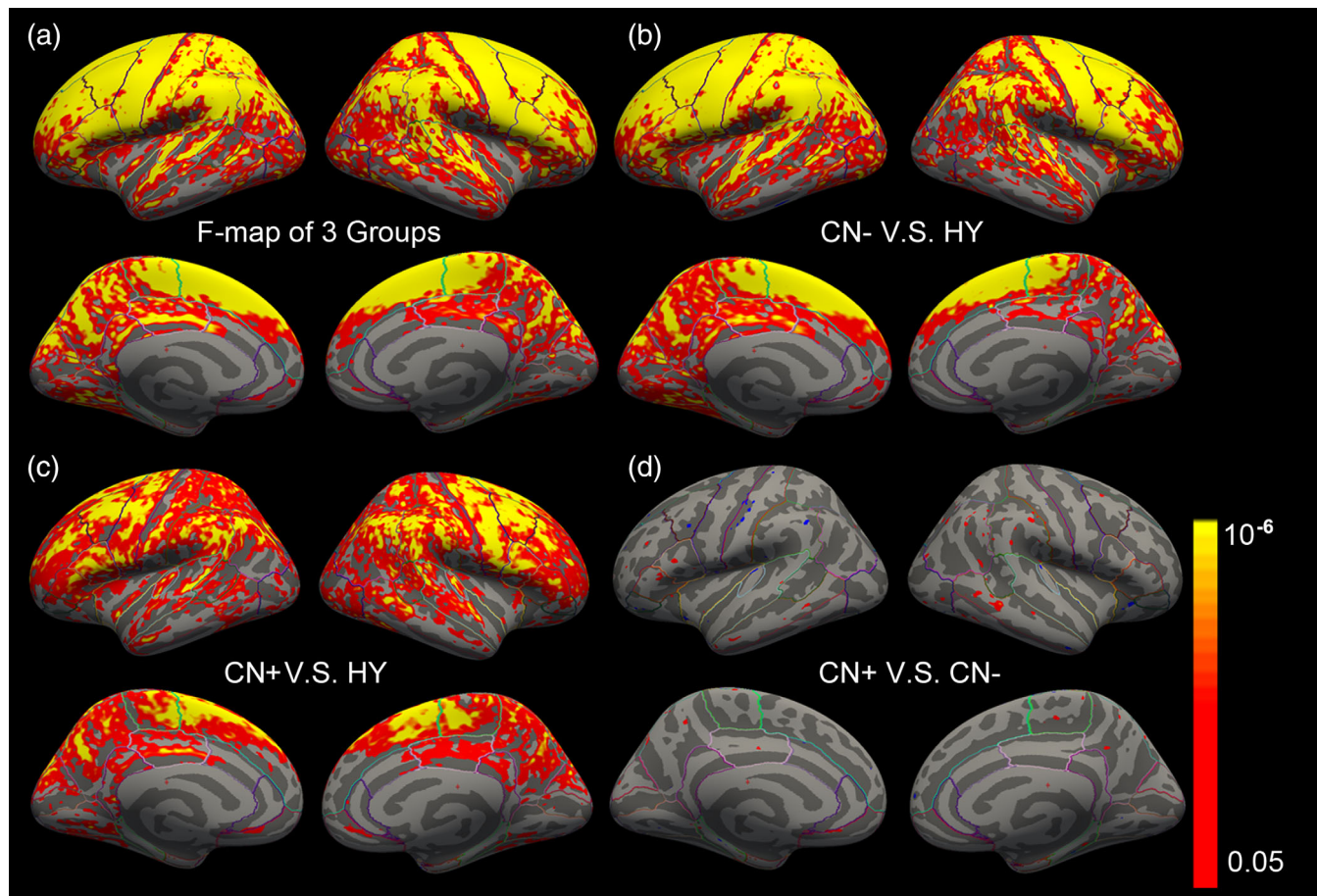


FIGURE 3 R^2 difference among groups in cortical regions. The color bar indicates the significance level with regions after the FDR correction ($p < .05$). p Values were projected onto the smoothed brain pial surface with the *Freelander* toolbox. (a) The p values of F-maps of one-way ANOVA analysis among three groups with FDR correction. (b) R^2 difference between the CN– and HY groups with FDR corrected. (c) R^2 difference between the CN+ and HY groups with FDR corrected. (d) R^2 difference between the CN– and CN+ groups with controlling the age under significance level $p < .01$ uncorrected

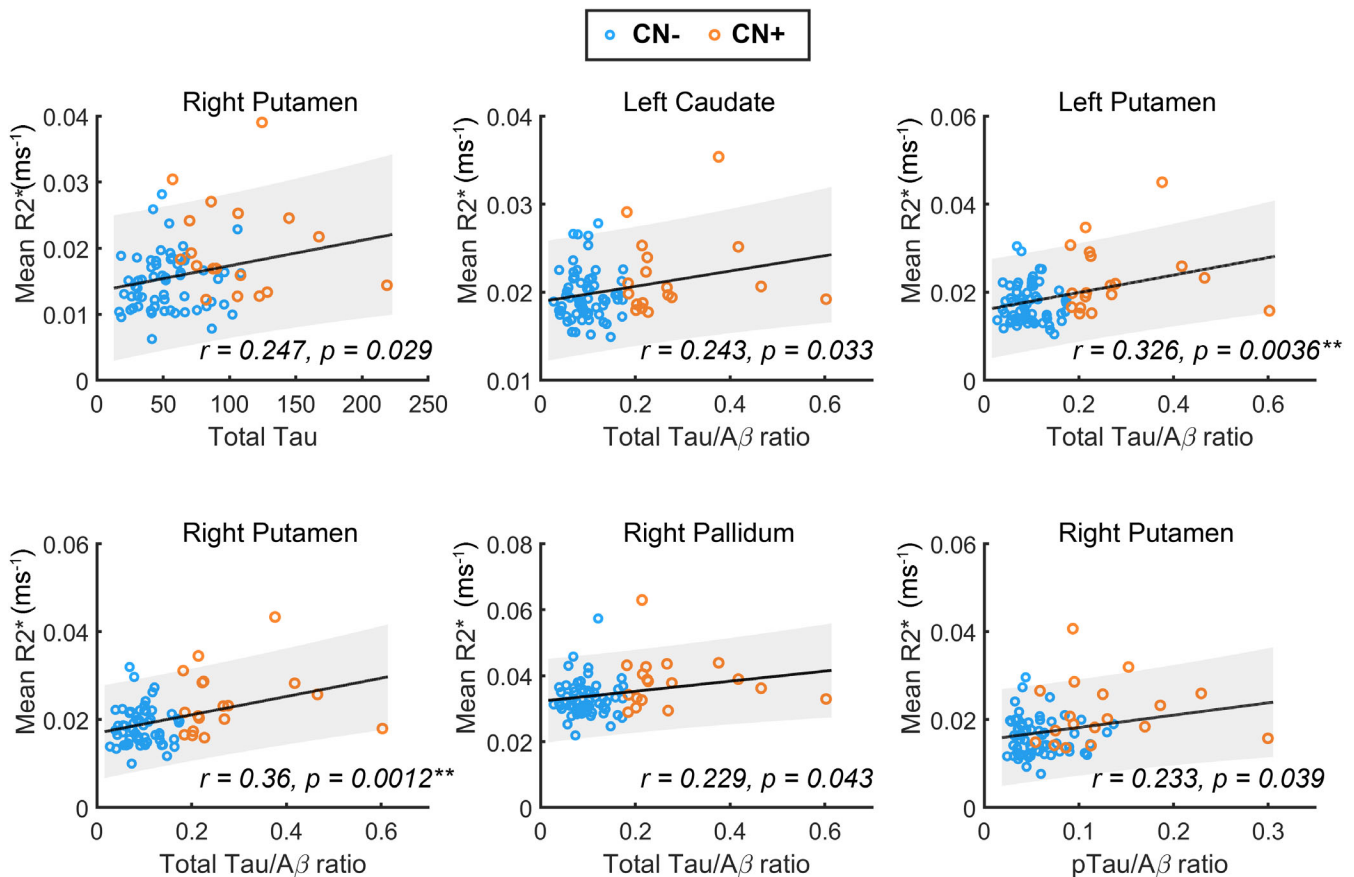


FIGURE 4 Correlations between subcortical R2* and cerebrospinal fluid (CSF) biomarkers in old groups. Partial correlation was applied to detect the relation between CSF biomarkers and subcortical R2* with controlling the age effects. Blue dots represent the CN- group and orange dots the CN+ group. R2* values are given in kilohertz (ms⁻¹); cerebrospinal fluid Total Tau levels are given in picogram per milliliter (pg/mL); ** indicates the correlations that survives with $p < .05$ FDR correction

adjusted $p = .0083$), and right putamen ($r = 0.360$, uncorrected $p = .0012$, FDR-adjusted $p = .0042$) with FDR correction $p < .05$. There were also some trend toward significant correlations for other regions that did not survive with FDR correction. More specifically, the R2* value of right putamen was correlated with CSF total Tau with a positive slope ($r = 0.247$, uncorrected $p = .0291$). R2* values were significantly correlated with CSF T-tau/A β ratio in the left caudate ($r = .243$, uncorrected $p = .0325$), and right pallidum ($r = .233$, uncorrected $p = .0434$). The R2* value of the right putamen was significantly correlated with CSF pTau/A β ratio with a positive slope ($r = 0.233$, uncorrected $p = .039$).

Significant negative correlations were found between neuropsychological performance and R2* value of several subcortical regions ($p < .05$, uncorrected; Figure 5). The total JoLO score was significantly negatively correlated R2* value of the left pallidum ($r = -0.261$, $p = .027$), right putamen ($r = -0.252$, $p = .033$), and right pallidum ($r = -0.326$, $p = .0053$). The Rey-O immediate recall score was significantly negatively correlated with R2* values of the left accumbens ($r = -0.253$, $p = .032$). Rey-O delayed recall score was negatively correlated with R2* value of left putamen ($r = -0.251$, $p = .035$; Figure 5).

3.3 | Group comparison of quantitative R1 and correlation with CSF biomarkers and cognitive tests

In contrast to differences found in R2* between the three groups, one-way ANOVA analysis revealed no significant differences in R1 between the HY, CN-, and CN+ groups in the subcortical and cortical regions after multiple comparison correction, although right accumbens showed an uncorrected group effect ($F = 3.67$, $p = .028$, uncorrected). In contrast to correlations seen with R2*, no significant correlations were found between regions showing significant group effects in R1 and cognitive measurements after controlling for the effect of age. No significant correlations were found between R1 and age.

4 | DISCUSSION

In this study, we investigated quantitative MR relaxation rates, R2* and R1, between healthy young and cognitively normal older subjects with positive (i.e., CN+) and negative (i.e., CN-) CSF biomarkers of AD pathology, respectively. We found widespread differences of R2*

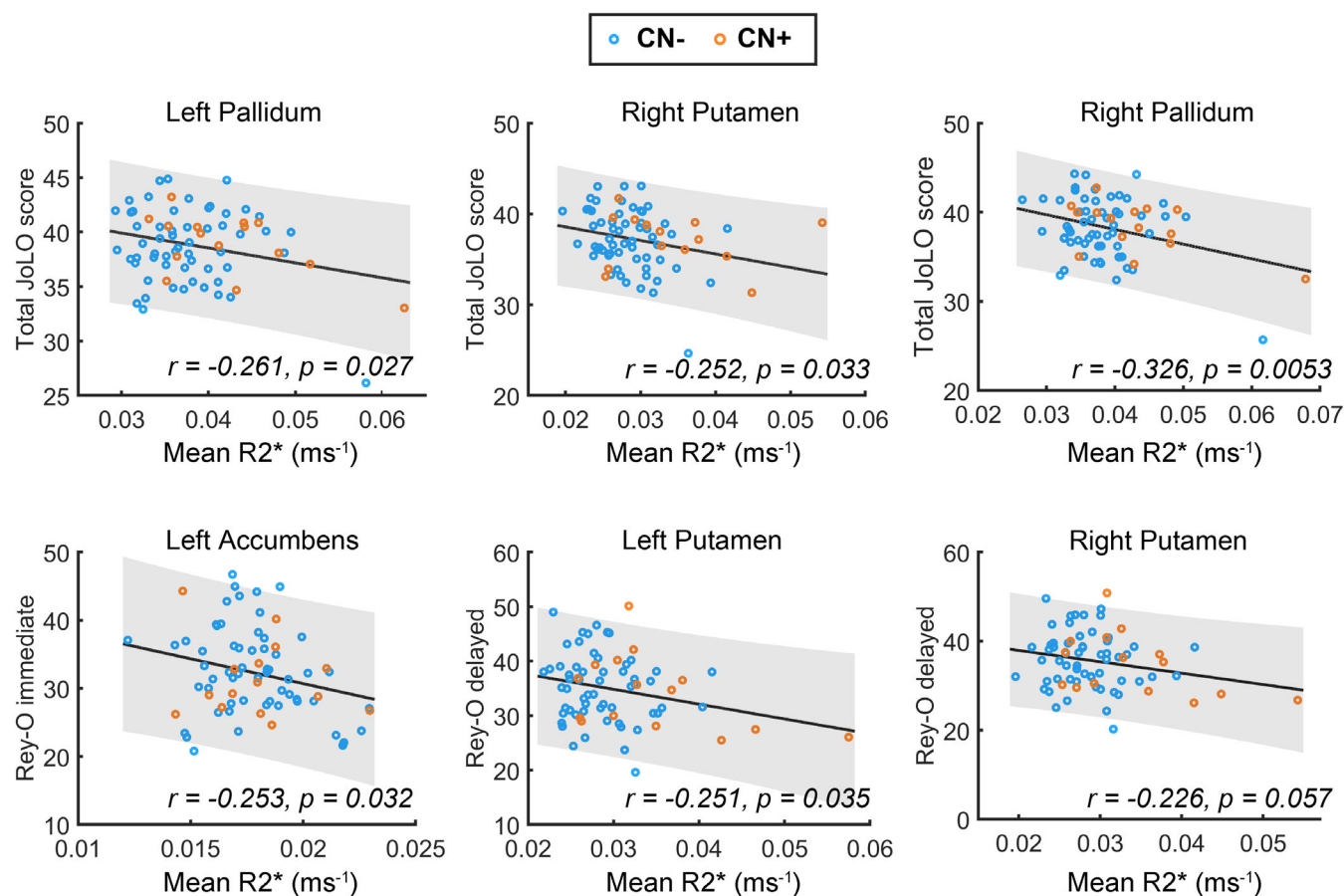


FIGURE 5 Correlations between subcortical R2* and cognitive scores in CN- and CN+ groups. Partial correlation was applied to detect the relationship between cognitive scores (JoLO and RCFT) and subcortical R2* in old group (CN- and CN+ combined) controlling for age effects (uncorrected *p*-value). Blue dots represent the CN- group and orange dots the CN+ group. R2* values are given in kilohertz (ms⁻¹); Rey-O immediate: Immediate free recall score of Rey Figure Test; Rey-O delayed: Delay recall score of Rey Figure Test; JoLO: judgment of line orientation test

in the cortex among HY, CN-, and CN+, primarily due to aging-related differences between HY and the two older groups. More interestingly, when comparing CN- with CN+ to study the effects of AD pathology in the older subjects, we found significantly increased R2* in the basal ganglia regions in the CN+ group; to our knowledge, this finding has not been previously reported previously in asymptomatic AD (i.e., CN+) subjects. We further found that R2* values in some basal ganglia regions correlated primarily with CSF total Tau level and total Tau to A β ratio but not with raw A β level in the older subjects. The elevated R2* in some basal ganglia regions were found to have neurocognitive implications as shown by their significant correlation with neuropsychological performance primarily related to visuospatial functions.

While R2* values in the white matter might have a significant contribution from myelin content, R2* values in the basal ganglia regions are primarily driven by iron content (Langkammer et al., 2010). Therefore, it is reasonable to infer that the increased R2* values in the basal ganglia regions in the asymptomatic AD are due to iron over-accumulation in these regions and that it could play a role in the early

pathophysiology of AD, consistent with findings in animal and post-mortem studies (El Tayara et al., 2006; House et al., 2007).

Widespread differences in R2* in many cortical and subcortical regions between HY and the older groups are consistent with previous reports of increased iron deposition with age (Callaghan et al., 2014; Ghadery et al., 2015). However, it is also noteworthy that no R2* changes in either the left or right thalamus were found in our study, consistent with previous reports (Aquino et al., 2009; Ghadery et al., 2015) and the general recognition that the thalamus is relatively spared from iron accumulation in healthy aging (Bartzokis et al., 1997; Hallgren & Sourander, 1958).

Our results demonstrate, for the first time, increased R2* in basal ganglia regions in cognitively normal subjects with positive AD pathology compared to those with negative AD pathology. These findings extend previous animal and postmortem studies in suggesting that iron accumulation occurs early in AD and could play a causal role in AD pathophysiology instead of being a downstream effect. Although the exact etiology and causal relationship between iron accumulation, A β and Tau in AD patients remain to be fully

uncovered, iron accumulation is closely linked to A β , Tau, and neuroinflammation. It is either possible that positive AD pathology initiates iron accumulation, or that people with higher brain iron are more likely to develop positive AD pathology. A β plaques can directly initiate the accumulation of iron or directly through the activation of microglia. Several previous studies have demonstrated A β and tau depositions in basal ganglia in asymptomatic and symptomatic AD patients (Chetelat et al., 2013; Rowe et al., 2008). Iron deposits have been found to colocalize with amyloid plaques and neurofibrillary tangles in transgenic mouse models of AD (Falangola et al., 2005) and patients with AD (Bulk et al., 2018; Spotorno et al., 2020; van Bergen et al., 2016). Iron has also been found to colocalize with activated microglia around and presumably activated by amyloid plaques (Zeineh et al., 2015). Conversely, iron accumulation in the brain is a hallmark of aging, which is the greatest risk factor for AD. Some authors even suggest that the pathophysiological mechanisms underlying the role of aging on the onset of AD are closely related to brain iron and oxidative stress (Bonda et al., 2010; Nnah & Wessling-Resnick, 2018; Pratico, 2008). And there is evidence that iron aggravates A β accumulation (Edler et al., 2021; Zecca et al., 2004). In a study of the brain of fly where the iron levels was manipulated using iron-selective chelating compound and RNAi-mediated knockdown of endogenous ferritin, higher iron levels have been found to slow the progression of the A β peptide from an unstructured conformation to the ordered cross- β fibrils, which would lead to aggregation of A β plaque and enhances A β toxicity (Liu et al., 2011). In cultured primary cortical neurons and the brain of APP/PS1 AD-model mice, iron overload was found to increase the production of amyloidogenic kunitz protease inhibitor amyloid precursor protein (KPI-APP) and A β (Becerril-Ortega et al., 2014). In addition, during brain ageing and iron accumulation, iron is partially converted from stable and soluble form (ferritin) to higher reactivity form of hemosiderin and other oxyhydroxide derivatives that might perturb the cellular environment and lead to neuroinflammation (Zecca et al., 2004). Several recent studies also reported that iron is associated with tau and mediates the effect of tau on brain volume and cognitive decline (Ayton et al., 2020; Spotorno et al., 2020). It is therefore possible that participants with higher brain iron content are at higher risk of developing AD. Conversely, it is also possible that AD pathology might promote over-accumulation of brain iron. There are also studies proposing that iron accumulations in the brain might be associated with the myelin loss process (Bartzokis, 2011; Khattar et al., 2021). Future studies are warranted to further investigate the relationships between brain morphology changes, AD pathology, and iron deposition. For example, longitudinal studies would be required to investigate whether AD biomarker-negative individuals with higher subcortical R2* are at a higher risk of becoming biomarker-positive over time. Iron over-accumulation has been reported in temporal and parietal regions among individuals with symptomatic AD (Damulina et al., 2020; Griffiths & Crossman, 1993; House et al., 2008; Tao et al., 2014), but we did not find significant R2* differences between CN+ and CN- groups in these or other cortical regions. This discrepancy may be explained by the very early stage of AD pathology in

our CN+ participants. This may indicate that increased R2* value in the older group may be related to the A β and total tau deposition levels and how iron overload interacts with other pathophysiological processes in leading to cognitive impairment.

We found significant negative correlations between the R2* values of basal ganglia areas and cognitive performance. While basal ganglia have traditionally been considered primarily in the context of motor functions, structural connectivity studies have revealed that basal ganglia loops with widespread connections with cortical regions (Karnath et al., 2002; Umarova et al., 2010). These are part of the fronto-basal ganglia-parieto-cerebellar pathway, which is a key part of the visuospatial attention network (Karnath et al., 2002; Umarova et al., 2010). The cognitive tests examined in the current study included Rey Complex Figure Test, which measures visuospatial constructional ability and nonverbal memory skills (Shin et al., 2006) and Judgment of Line Orientation, which measures visuo-perceptual functions. We found a negative association of R2* with visuospatial functions, which are declining in healthy aging and early stages of AD (Darnai et al., 2017; Trojano & Gainotti, 2016). Interestingly, visuospatial deficits may also be detected at the pre-clinical stage of AD (Iachini et al., 2009; Wilson et al., 2011). Taken together, these results suggested that the increased iron deposition as measured by R2* in the basal ganglia regions may be related to decline of visuospatial and memory functions in the early stages of AD.

4.1 | Changes in quantitative R1 mapping

Quantitative R1 value is thought to be related to changes in tissue myelination and cellularity (Callaghan et al., 2014; Yeatman et al., 2014). In current study, we found no significant R1 differences between the older and younger control groups. This may be because the age-related changes of R1 in brain regions follow an inverted U-curve, with increasing R1 values up to around age 40 followed up by a decreasing trend (Carradus et al., 2020; Yeatman et al., 2014). The R1 decline with age after 40 years is mirror-symmetric with the R1 increase during development (Yeatman et al., 2014). In our current study, the age of most of the younger group was between 21 and 30, and the age of the older group ranged from 60 to 80. These age ranges are at the two ends of the inverted U-curve, likely resulting in the lack of differences. Future studies with more subjects between 30 and 60 years of age might provide more information on the non-linear pattern of T1 changes across the adult lifespan.

4.2 | Limitations and further considerations

Several methodological issues need to be addressed. First, we used CSF protein levels as evidence of AD pathology, but unlike PET, CSF biomarkers provide no information about the regional accumulation of AD pathology. It will be interesting to study whether increased R2* in

the basal ganglia is associated with local levels of AD pathology in these regions. Future studies incorporating advanced amyloid and tau PET imaging would allow exploration of R2* signal relative to spatial patterns of A β and Tau deposition. Second, in the imaging processing part, we used double-flip angle 2D EPI sequences to correct the B1 transmission inhomogeneity. The 2D EPI imaging may be affected by the out-of-bandwidth magnetization contamination and slice profile distortions (Bouhrara & Bonny, 2012). We used a mono-exponential fit method to calculate the R2*. Future advanced models incorporating the non-Gaussian noise models could help to get more accurate R2* mapping (Balbastre et al., 2021). Third, our current study focused on healthy older participants 60–80 years of age and younger controls 21–30 years of age. The inclusion of individuals between 30 and 60 years would provide important information about brain microstructures across the life span. Also, there are only 18 participants total with only two male participants in CN+ group due to the natural low prevalence of positive AD pathology in cognitively normal individuals in the current age-range (Jansen et al., 2015) and high proportion of female volunteers in our cohort. Future studies with larger sample size and better gender balance will be needed to increase statistical power. Fourth, the correlations between the R2* value of subcortical regions and cognitive performance were not corrected by multiple comparisons. Caution must be exercised in interpreting these correlations. These exploratory results need further confirmation in larger and independent data sets in further study. Additionally, the APOE-e4 might be a risk factor that influences the brain iron depositions in normal aging and AD pathology, however, we did not have the APOE-e4 gene status at the time of analyses. The relationships between the APOE status and iron depositions in the early asymptomatic stages of AD need to be further studied. Lastly, our study is cross-sectional. Future studies incorporating longitudinal data are needed for providing more specific information about how brain microstructure changes during the aging process and in the transition from asymptomatic to symptomatic stages of AD.

In conclusion, we found significantly increased R2* values in subcortical brain regions in individuals with asymptomatic AD, suggesting iron over-accumulation in early stages of disease evolution. These findings lead us to conclude that quantitative MR may be able to provide a sensitive biomarker for detecting early microstructural brain changes in AD, justifying further investigations with longitudinal study designs.

ACKNOWLEDGEMENTS

The study was supported by Goizueta Foundation and National Institutes of Health (R21AG064405, R01AG070937, R01AG072603, P30AG066511).

CONFLICT OF INTEREST STATEMENT

The authors declare no conflict of interest.

DATA AVAILABILITY STATEMENT

The data that support the findings of this study are available from the corresponding author upon reasonable request.

ORCID

Deqiang Qiu  <https://orcid.org/0000-0001-8375-1755>

REFERENCES

- Aquino, D., Bizzi, A., Grisoli, M., Garavaglia, B., Bruzzone, M. G., Nardocci, N., Savoiardo, M., & Chiapparini, L. (2009). Age-related iron deposition in the basal ganglia: Quantitative analysis in healthy subjects. *Radiology*, 252(1), 165–172. <https://doi.org/10.1148/radiol.2522081399>
- Ayton, S., Wang, Y., Diouf, I., Schneider, J. A., Brockman, J., Morris, M. C., & Bush, A. I. (2020). Brain iron is associated with accelerated cognitive decline in people with Alzheimer pathology. *Molecular Psychiatry*, 25(11), 2932–2941. <https://doi.org/10.1038/s41380-019-0375-7>
- Balbastre, Y., Brudfors, M., Azzarito, M., Lambert, C., Callaghan, M. F., & Ashburner, J. (2021). Model-based multi-parameter mapping. *Medical Image Analysis*, 73, 102149. <https://doi.org/10.1016/j.media.2021.102149>
- Bartzokis, G. (2011). Alzheimer's disease as homeostatic responses to age-related myelin breakdown. *Neurobiology of Aging*, 32(8), 1341–1371. <https://doi.org/10.1016/j.neurobiolaging.2009.08.007>
- Bartzokis, G., Beckson, M., Hance, D. B., Marx, P., Foster, J. A., & Marder, S. R. (1997). MR evaluation of age-related increase of brain iron in young adult and older normal males. *Magnetic Resonance Imaging*, 15(1), 29–35. [https://doi.org/10.1016/s0730-725x\(96\)00234-2](https://doi.org/10.1016/s0730-725x(96)00234-2)
- Becerril-Ortega, J., Bordji, K., Freret, T., Rush, T., & Buisson, A. (2014). Iron overload accelerates neuronal amyloid-beta production and cognitive impairment in transgenic mice model of Alzheimer's disease. *Neurobiology of Aging*, 35(10), 2288–2301. <https://doi.org/10.1016/j.neurobiolaging.2014.04.019>
- Benton, A. L., Sivan, A. B., Hamsner, K. d., Varney, N. R., & Spreen, O. (1994). *Contributions to neuropsychological assessment: A clinical manual*. Oxford University Press.
- Bonda, D. J., Wang, X., Perry, G., Nunomura, A., Tabaton, M., Zhu, X., & Smith, M. A. (2010). Oxidative stress in Alzheimer disease: A possibility for prevention. *Neuropharmacology*, 59(4–5), 290–294. <https://doi.org/10.1016/j.neuropharm.2010.04.005>
- Bouhrara, M., & Bonny, J. M. (2012). B(1) mapping with selective pulses. *Magnetic Resonance in Medicine*, 68(5), 1472–1480. <https://doi.org/10.1002/mrm.24146>
- Bulk, M., Kenkhuis, B., van der Graaf, L. M., Goeman, J. J., Natte, R., & van der Weerd, L. (2018). Postmortem T2*- weighted MRI imaging of cortical iron reflects severity of Alzheimer's disease. *Journal of Alzheimer's Disease*, 65(4), 1125–1137. <https://doi.org/10.3233/JAD-180317>
- Callaghan, M. F., Freund, P., Draganski, B., Anderson, E., Cappelletti, M., Chowdhury, R., Diedrichsen, J., Fitzgerald, T.H., Smittenaar, P., Helms, G., Lutti, & Weiskopf, N. (2014). Widespread age-related differences in the human brain microstructure revealed by quantitative magnetic resonance imaging. *Neurobiology of Aging*, 35(8), 1862–1872. <https://doi.org/10.1016/j.neurobiolaging.2014.02.008>
- Carradus, A. J., Mouglin, O., Hunt, B. A. E., Tewarie, P. K., Geades, N., Morris, P. G., Done Brookes, M.J., Gowland, P.A., & Madan, C. R. (2020). Age-related differences in myeloarchitecture measured at 7 T. *Neurobiology of Aging*, 96, 246–254. <https://doi.org/10.1016/j.neurobiolaging.2020.08.009>
- Chetelat, G., La Joie, R., Villain, N., Perrotin, A., de La Sayette, V., Eustache, F., & Vandenberghe, R. (2013). Amyloid imaging in cognitively normal individuals, at-risk populations and preclinical Alzheimer's disease. *Neuroimage: Clinical*, 2, 356–365. <https://doi.org/10.1016/j.nicl.2013.02.006>
- Collingwood, J. F., Mikhaylova, A., Davidson, M., Batich, C., Streit, W. J., Terry, J., & Dobson, J. (2005). In situ characterization and mapping of iron compounds in Alzheimer's disease tissue. *Journal of Alzheimer's Disease*, 7(4), 267–272. <https://doi.org/10.3233/jad-2005-7401>

- Cunningham, C. H., Pauly, J. M., & Nayak, K. S. (2006). Saturated double-angle method for rapid B1+ mapping. *Magnetic Resonance in Medicine*, 55(6), 1326–1333. <https://doi.org/10.1002/mrm.20896>
- Damulina, A., Pirpamer, L., Soellradl, M., Sackl, M., Tinauer, C., Hofer, E., Enzinger, C., Gesierich, B., Duering, M., Ropele, S., Schmidt, R., & Langkammer, C. (2020). Cross-sectional and longitudinal assessment of brain iron level in Alzheimer disease using 3-T MRI. *Radiology*, 296(3), 619–626. <https://doi.org/10.1148/radiol.2020192541>
- Darnai, G., Nagy, S. A., Horvath, R., Acs, P., Perlaki, G., Orsi, G., Kovacs, N., Altbacker, A., Plozer, E., Tenyi, D., Weintraut, R., Schwarcz, A., John, F., Varga, E., Bereczkei, T., Clemens, Z., Komoly, & Janszky, J. (2017). Iron concentration in deep gray matter structures is associated with worse visual memory performance in healthy young adults. *Journal of Alzheimer's Disease*, 59(2), 675–681. <https://doi.org/10.3233/JAD-170118>
- Daugherty, A. M., & Raz, N. (2015). Appraising the role of iron in brain aging and cognition: Promises and limitations of MRI methods. *Neuropsychology Review*, 25(3), 272–287. <https://doi.org/10.1007/s11065-015-9292-y>
- Deoni, S. C., Rutt, B. K., & Peters, T. M. (2003). Rapid combined T1 and T2 mapping using gradient recalled acquisition in the steady state. *Magnetic Resonance in Medicine*, 49(3), 515–526.
- Doody, R. S., Thomas, R. G., Farlow, M., Iwatsubo, T., Vellas, B., Joffe, S., Kieburtz, K., Raman, R., Sun, X., Aisen, P.S., Siemers, E., Liu-Seifert, H., & Solanezumab Study, G. (2014). Phase 3 trials of solanezumab for mild-to-moderate Alzheimer's disease. *The New England Journal of Medicine*, 370(4), 311–321. <https://doi.org/10.1056/NEJMoa1312889>
- Edler, M. K., Mhatre-Winters, I., & Richardson, J. R. (2021). Microglia in aging and Alzheimer's disease: A comparative species review. *Cell*, 10(5), 1138.
- El Tayara, N. E. T., Delatour, B., Le Cudennec, C., Guégan, M., Volk, A., & Dhenain, M. (2006). Age-related evolution of amyloid burden, iron load, and MR relaxation times in a transgenic mouse model of Alzheimer's disease. *Neurobiology of Disease*, 22(1), 199–208.
- Fagan, A. M., Roe, C. M., Xiong, C., Mintun, M. A., Morris, J. C., & Holtzman, D. M. (2007). Cerebrospinal fluid tau/beta-amyloid(42) ratio as a prediction of cognitive decline in nondemented older adults. *Archives of Neurology*, 64(3), 343–349. <https://doi.org/10.1001/archneur.64.3.noc60123>
- Falangola, M. F., Lee, S.-P., Nixon, R. A., Duff, K., & Helpner, J. A. (2005). Histological co-localization of iron in A β plaques of PS/APP transgenic mice. *Neurochemical Research*, 30(2), 201–205.
- Ghadery, C., Pirpamer, L., Hofer, E., Langkammer, C., Petrovic, K., Loitfelder, M., Schwingenschuh, P., Seiler, S., Duering, M., Jouvent, E., Schmidt, H., Fazekas, F., Mangin, J.F., Chabriet, H., Dichgans, M., Ropele, S., & Schmidt, R. (2015). R2* mapping for brain iron: Associations with cognition in normal aging. *Neurobiology of Aging*, 36(2), 925–932. <https://doi.org/10.1016/j.neurobiolaging.2014.09.013>
- Goetz, M. E., Hanfelt, J. J., John, S. E., Bergquist, S. H., Loring, D. W., Quyyumi, A., Clifford, G.D., Vaccarino, V., Goldstein, F., Johnson Nd, T.M., Kuerston, R., Marcus, M., Levey, A.I., & Lah, J. J. (2019). Rationale and design of the emory healthy aging and emory healthy brain studies. *Neuroepidemiology*, 53(3–4), 187–200. <https://doi.org/10.1159/000501856>
- Griffiths, P. D., & Crossman, A. R. (1993). Distribution of iron in the basal ganglia and neocortex in postmortem tissue in Parkinson's disease and Alzheimer's disease. *Dementia*, 4(2), 61–65. <https://doi.org/10.1159/000107298>
- Haacke, E. M., Cheng, N. Y., House, M. J., Liu, Q., Neelavalli, J., Ogg, R. J., Khan, A., Ayaz, M., Kirsch, W., & Obenaus, A. (2005). Imaging iron stores in the brain using magnetic resonance imaging. *Magnetic Resonance Imaging*, 23(1), 1–25. <https://doi.org/10.1016/j.mri.2004.10.001>
- Haider, L., Simeonidou, C., Steinberger, G., Hametner, S., Grigoriadis, N., Deretzi, G., Kovacs, G. G., Kutzelnigg, A., Lassmann, H., & Frischer, J. M. (2014). Multiple sclerosis deep grey matter: The relation between demyelination, neurodegeneration, inflammation and iron. *Journal of Neurology, Neurosurgery, and Psychiatry*, 85(12), 1386–1395.
- Hallgren, B., & Sourander, P. (1958). The effect of age on the non-haemin iron in the human brain. *Journal of Neurochemistry*, 3(1), 41–51. <https://doi.org/10.1111/j.1471-4159.1958.tb12607.x>
- House, M. J., St Pierre, T. G., Kowdley, K. V., Montine, T., Connor, J., Beard, J., Berger, J., Siddaiah, N., Shankland, E., & Jin, L. W. (2007). Correlation of proton transverse relaxation rates (R2) with iron concentrations in postmortem brain tissue from Alzheimer's disease patients. *Magnetic Resonance in Medicine*, 57(1), 172–180. <https://doi.org/10.1002/mrm.21118>
- House, M. J., St Pierre, T. G., & McLean, C. (2008). 1.4T study of proton magnetic relaxation rates, iron concentrations, and plaque burden in Alzheimer's disease and control postmortem brain tissue. *Magnetic Resonance in Medicine*, 60(1), 41–52. <https://doi.org/10.1002/mrm.21586>
- Iachini, I., Iavarone, A., Senese, V. P., Ruotolo, F., & Ruggiero, G. (2009). Visuospatial memory in healthy elderly, AD and MCI: A review. *Current Aging Science*, 2(1), 43–59. <https://doi.org/10.2174/1874609810902010043>
- Jack, C. R., Jr., Bennett, D. A., Blennow, K., Carrillo, M. C., Dunn, B., Haeberlein, S. B., Holtzman, D.M., Jagust, W., Jessen, F., Karlawish, J., Liu, E., Molinuevo, J.L., Montine, T., Phelps, C., Rankin, K.P., Rowe, C.C., Scheltens, P., Siemers, E., Snyder, H.M., & Contributors. (2018). NIA-AA research framework: Toward a biological definition of Alzheimer's disease. *Alzheimers Dement*, 14(4), 535–562. <https://doi.org/10.1016/j.jalz.2018.02.018>
- Jansen, W. J., Ossenkoppele, R., Knol, D. L., Tijms, B. M., Scheltens, P., Verhey, F. R. J., Grp, A. B. S. (2015). Prevalence of cerebral amyloid pathology in persons without dementia: a meta-analysis. *JAMA*, 313(19), 1924–1938. <https://doi.org/10.1001/jama.2015.4668>
- Karnath, H. O., Himmelbach, M., & Rorden, C. (2002). The subcortical anatomy of human spatial neglect: Putamen, caudate nucleus and pulvinar. *Brain*, 125(Pt 2), 350–360. <https://doi.org/10.1093/brain/awf032>
- Khattar, N., Triebswetter, C., Kiely, M., Ferrucci, L., Resnick, S. M., Spencer, R. G., & Bouhrara, M. (2021). Investigation of the association between cerebral iron content and myelin content in normative aging using quantitative magnetic resonance neuroimaging. *NeuroImage*, 239, 118267. <https://doi.org/10.1016/j.neuroimage.2021.118267>
- Langkammer, C., Krebs, N., Goessler, W., Scheurer, E., Ebner, F., Yen, K., Fazekas, F., & Ropele, S. (2010). Quantitative MR imaging of brain iron: A postmortem validation study. *Radiology*, 257(2), 455–462. <https://doi.org/10.1148/radiol.10100495>
- Lin, Q., Shahid, S., Hone-Blanchet, A., Levey, A., Lah, J., Crosson, B., & Qiu, D. (2019). Brain microstructure changes in healthy aging revealed by quantitative multi-parametric MRI. *Proceedings of the International Society for Magnetic Resonance in Medicine*, 28, 2627.
- Liu, B., Moloney, A., Meehan, S., Morris, K., Thomas, S. E., Serpell, L. C., Hider, R., Marciniak, S.J., Lomas, D.A., & Crowther, D. C. (2011). Iron promotes the toxicity of amyloid beta peptide by impeding its ordered aggregation. *The Journal of Biological Chemistry*, 286(6), 4248–4256. <https://doi.org/10.1074/jbc.M110.158980>
- Lutti, A., Dick, F., Sereno, M. I., & Weiskopf, N. (2014). Using high-resolution quantitative mapping of R1 as an index of cortical myelination. *NeuroImage*, 93(Pt 2), 176–188. <https://doi.org/10.1016/j.neuroimage.2013.06.005>
- Mills, E., Dong, X. P., Wang, F., & Xu, H. (2010). Mechanisms of brain iron transport: Insight into neurodegeneration and CNS disorders. *Future Medicinal Chemistry*, 2(1), 51–64.
- Mintun, M. A., Larossa, G. N., Sheline, Y. I., Dence, C. S., Lee, S. Y., Mach, R. H., Klunk, W.E., Mathis, C.A., DeKosky, S.T., & Morris, J. C. (2006). [11C]PIB in a nondemented population: Potential antecedent marker of Alzheimer disease. *Neurology*, 67(3), 446–452. <https://doi.org/10.1212/01.wnl.0000228230.26044.a4>

- Nasreddine, Z. S., Phillips, N. A., Bedirian, V., Charbonneau, S., Whitehead, V., Collin, I., Cummings, J.L., & Chertkow, H. (2005). The Montreal cognitive assessment, MoCA: A brief screening tool for mild cognitive impairment. *Journal of the American Geriatrics Society*, 53(4), 695–699. <https://doi.org/10.1111/j.1532-5415.2005.53221.x>
- Nnah, I. C., & Wessling-Resnick, M. (2018). Brain iron homeostasis: A focus on microglial iron. *Pharmaceuticals (Basel)*, 11(4), 129. <https://doi.org/10.3390/ph11040129>
- Osterrieth, P. A. (1944). Le test de copie d'une figure complexe; contribution a l'etude de la perception et de la memoire. *Archives de Psychologie*, 30, 206–356.
- Pratico, D. (2008). Oxidative stress hypothesis in Alzheimer's disease: A reappraisal. *Trends in Pharmacological Sciences*, 29(12), 609–615. <https://doi.org/10.1016/j.tips.2008.09.001>
- Rowe, C. C., Ackerman, U., Browne, W., Mulligan, R., Pike, K. L., O'Keefe, G., Tochon-Danguy, H., Chan, G., Berlangieri, S.U., Jones, G., Dickinson-Rowe, K.L., Kung, H.P., Zhang, W., Kung, M.P., Skovronsky, D., Dyrks, T., Holl, G., Krause, S., M., Lehman, L., & Villemagne, V. L. (2008). Imaging of amyloid beta in Alzheimer's disease with 18F-BAY94-9172, a novel PET tracer: Proof of mechanism. *The Lancet: Neurology*, 7(2), 129–135. [https://doi.org/10.1016/S1474-4422\(08\)70001-2](https://doi.org/10.1016/S1474-4422(08)70001-2)
- Rowe, C. C., Bourgeat, P., Ellis, K. A., Brown, B., Lim, Y. Y., Mulligan, R., Jones, G., Maruff, P., Woodward, M., Price, R., Robins, P., Tochon-Danguy, H., O'Keefe, G., Pike, K.E., Yates, P., Szoek, C., Salvado, O., Macaulay, S.L., O'Meara, T., & Villemagne, V. L. (2013). Predicting Alzheimer disease with beta-amyloid imaging: Results from the Australian imaging, biomarkers, and lifestyle study of ageing. *Annals of Neurology*, 74(6), 905–913. <https://doi.org/10.1002/ana.24040>
- Salloway, S., Sperling, R., Fox, N. C., Blennow, K., Klunk, W., Raskind, M., Sabbagh, M., Honig, L.S., Porsteinsson, A.P., Ferris, S., Reichert, M., Ketter, N., Nejadnik, B., Guenzler, V., Miloslavsky, M., Wang, D., Lu, Y., Lull, J., Tudor, I.C., & Clinical Trial, I. (2014). Two phase 3 trials of bapineuzumab in mild-to-moderate Alzheimer's disease. *The New England Journal of Medicine*, 370(4), 322–333. <https://doi.org/10.1056/NEJMoa1304839>
- Sedlacik, J., Boelmans, K., Lobel, U., Holst, B., Siemonsen, S., & Fiehler, J. (2014). Reversible, irreversible and effective transverse relaxation rates in normal aging brain at 3T. *NeuroImage*, 84, 1032–1041. <https://doi.org/10.1016/j.neuroimage.2013.08.051>
- Selkoe, D. J. (1991). The molecular pathology of Alzheimer's disease. *Neuron*, 6(4), 487–498. [https://doi.org/10.1016/0896-6273\(91\)90052-2](https://doi.org/10.1016/0896-6273(91)90052-2)
- Shaw, L. M., Vanderstichele, H., Knapiak-Czajka, M., Clark, C. M., Aisen, P. S., Petersen, R. C., Blennow, K., Soares, H., Simon, A., Lewczuk, P., Dean, R., Siemers, E., Potter, W., Lee, V.M., Trojanowski, J.Q., & Alzheimer's Disease Neuroimaging. (2009). Cerebrospinal fluid biomarker signature in Alzheimer's disease neuroimaging initiative subjects. *Annals of Neurology*, 65(4), 403–413. <https://doi.org/10.1002/ana.21610>
- Shin, M. S., Park, S. Y., Park, S. R., Seol, S. H., & Kwon, J. S. (2006). Clinical and empirical applications of the Rey-Osterrieth complex figure test. *Nature Protocols*, 1(2), 892–899. <https://doi.org/10.1038/nprot.2006.115>
- Sigalovsky, I. S., Fischl, B., & Melcher, J. R. (2006). Mapping an intrinsic MR property of gray matter in auditory cortex of living humans: A possible marker for primary cortex and hemispheric differences. *NeuroImage*, 32(4), 1524–1537. <https://doi.org/10.1016/j.neuroimage.2006.05.023>
- Smith, M. A., Harris, P. L., Sayre, L. M., & Perry, G. (1997). Iron accumulation in Alzheimer disease is a source of redox-generated free radicals. *Proceedings of the National Academy of Sciences of the United States of America*, 94(18), 9866–9868. <https://doi.org/10.1073/pnas.94.18.9866>
- Spotorno, N., Acosta-Cabrero, J., Stomrud, E., Lampinen, B., Strandberg, O. T., van Westen, D., & Hansson, O. (2020). Relationship between cortical iron and tau aggregation in Alzheimer's disease. *Brain*, 143(5), 1341–1349. <https://doi.org/10.1093/brain/awaa089>
- Stuber, C., Morawski, M., Schafer, A., Labadie, C., Wahnert, M., Leuze, C., Streicher, M., Barapatre, N., Reimann, K., Geyer, S., Spemann, D., & Turner, R. (2014). Myelin and iron concentration in the human brain: A quantitative study of MRI contrast. *NeuroImage*, 93(Pt 1), 95–106. <https://doi.org/10.1016/j.neuroimage.2014.02.026>
- Tao, Y., Wang, Y., Rogers, J. T., & Wang, F. (2014). Perturbed iron distribution in Alzheimer's disease serum, cerebrospinal fluid, and selected brain regions: A systematic review and meta-analysis. *Journal of Alzheimer's Disease*, 42(2), 679–690. <https://doi.org/10.3233/JAD-140396>
- Todorich, B., Pasquini, J. M., Garcia, C. I., Paez, P. M., & Connor, J. R. (2009). Oligodendrocytes and myelination: The role of iron. *Glia*, 57(5), 467–478. <https://doi.org/10.1002/glia.20784>
- Trojano, L., & Gainotti, G. (2016). Drawing disorders in Alzheimer's disease and other forms of dementia. *Journal of Alzheimer's Disease*, 53(1), 31–52.
- Umarova, R. M., Saur, D., Schnell, S., Kaller, C. P., Vry, M. S., Glauche, V., Rijntjes, M., Hennig, J., Kiselev, V., & Weiller, C. (2010). Structural connectivity for visuospatial attention: Significance of ventral pathways. *Cerebral Cortex*, 20(1), 121–129. <https://doi.org/10.1093/cercor/bhp086>
- van Bergen, J. M., Li, X., Hua, J., Schreiner, S. J., Steininger, S. C., Quevenco, F. C., Wyss, M., Gietl, A.F., Treyer, V., Leh, S.E., Buck, F., Nitsch, R.M., Pruessmann, K.P., van Zijl, P.C., Hock, C., & Unschuld, P. G. (2016). Colocalization of cerebral iron with amyloid beta in mild cognitive impairment. *Scientific Reports*, 6, 35514. <https://doi.org/10.1038/srep35514>
- Vandenberghe, R., Adamczuk, K., Dupont, P., Laere, K. V., & Chetelat, G. (2013). Amyloid PET in clinical practice: Its place in the multidimensional space of Alzheimer's disease. *NeuroImage: Clinical*, 2, 497–511. <https://doi.org/10.1016/j.nicl.2013.03.014>
- Ward, R. J., Zucca, F. A., Duyn, J. H., Crichton, R. R., & Zecca, L. (2014). The role of iron in brain ageing and neurodegenerative disorders. *Lancet Neurology*, 13(10), 1045–1060. [https://doi.org/10.1016/S1474-4422\(14\)70117-6](https://doi.org/10.1016/S1474-4422(14)70117-6)
- Wilson, R. S., Leurgans, S. E., Boyle, P. A., & Bennett, D. A. (2011). Cognitive decline in prodromal Alzheimer disease and mild cognitive impairment. *Archives of Neurology*, 68(3), 351–356. <https://doi.org/10.1001/archneurol.2011.31>
- World Health Organization. (2015). *World report on ageing and health*. World Health Organization.
- Yeatman, J. D., Wandell, B. A., & Mezer, A. A. (2014). Lifespan maturation and degeneration of human brain white matter. *Nature Communications*, 5, 4932. <https://doi.org/10.1038/ncomms5932>
- Zecca, L., Youdim, M. B., Riederer, P., Connor, J. R., & Crichton, R. R. (2004). Iron, brain ageing and neurodegenerative disorders. *Nature Reviews: Neuroscience*, 5(11), 863–873. <https://doi.org/10.1038/nrn1537>
- Zeineh, M. M., Chen, Y., Kitzler, H. H., Hammond, R., Vogel, H., & Rutt, B. K. (2015). Activated iron-containing microglia in the human hippocampus identified by magnetic resonance imaging in Alzheimer disease. *Neurobiology of Aging*, 36(9), 2483–2500. <https://doi.org/10.1016/j.neurobiolaging.2015.05.022>

SUPPORTING INFORMATION

Additional supporting information can be found online in the Supporting Information section at the end of this article.

How to cite this article: Lin, Q., Shahid, S., Hone-Blanchet, A., Huang, S., Wu, J., Bisht, A., Loring, D., Goldstein, F., Levey, A., Crosson, B., Lah, J., & Qiu, D. (2023). Magnetic resonance evidence of increased iron content in subcortical brain regions in asymptomatic Alzheimer's disease. *Human Brain Mapping*, 44(8), 3072–3083. <https://doi.org/10.1002/hbm.26263>